Electron liquid at any degeneracy

R. G. Dandrea and N. W. Ashcroft
Laboratory of Atomic and Solid State Physics, Cornell University, Ithaca, New York 14853-2501

A. E. Carlsson
Department of Physics, Washington University, St. Louis, Missouri 63130

(Received 10 March 1986)

A unified theory is presented that describes the thermodynamic and dielectric properties of the electron liquid throughout the full range of thermal degeneracy: from the zero-temperature fully degenerate Fermi plasma to the high-temperature classical one-component plasma. Through an approximate inclusion of local-field corrections in the polarizability, results are obtained that are accurate up to intermediate values of the coupling strength. For future applications, closed-form parametrizations are presented for the thermodynamic and dielectric functions, as functions of density and temperature. The consequences of an increase in temperature on the plasmon dispersion and damping, on the energy-loss function, and on the pair-correlation function are also studied. We find that quantum effects can be observed in the short-range behavior of the pair-correlation function even for some plasmas that are conventionally classified as classical.

I. INTRODUCTION

An accurate description of a one-component Fermi plasma at any degree of degeneracy is a problem of both fundamental and practical significance. As demonstrated in Fig. 1, plasma states of matter for which the one-component plasma (OCP) serves as a standard model are certainly ubiquitous in nature. Although an enormous effort over the past three decades has been expended in obtaining an accurate theoretical description of both the zero-temperature fermion OCP (degenerate electron liquid) and the high-temperature classical OCP, only recently have attempts been made to quantify the intermediate degeneracy regime of the fermion plasma. The goal of this work is to present a unified theory capable of describing the thermodynamic and dielectric properties of the fermion plasma throughout a broad range of densities and temperatures: from a fully degenerate quantum plasma, to a nondegenerate classical plasma. In order that the theory be particularly applicable to electron liquids at metallic densities, which are not weakly coupled, local-field corrections to the random-phase approximation are included in an approximate manner. Through comparison with Monte Carlo results both at zero temperature and in the classical regime, we find that this procedure provides an accurate description of the fermion plasma up to intermediate coupling strengths. In order to enhance the utility of the results we obtain for practical applications, we present closed-form parametrizations[1] of both the free energy and dielectric function, as functions of density and temperature. For nearly degenerate plasmas, this parametrization leads to a convenient method for including finite-temperature effects which goes beyond the usual Sommerfeld expansion for the ideal fermion contributions to the thermodynamics. In a similar way, for nearly classical plasmas it provides a scheme for conveniently including quantum corrections that also goes beyond the standard Wigner-Kirkwood expansion, which is, in fact, an ill-defined expansion for the OCP.[2] As discussed below, we find that plasmas of intermediate degeneracy are inadequately described by low temperature or classical approximations. Although our results are applicable to

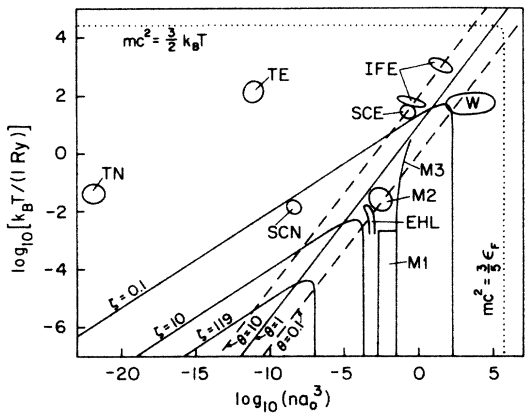

FIG. 1. Temperature-density plot for some plasmas for which the OCP serves as a model. The constant Θ lines denote the regions of degenerate behavior ($\Theta < 10$), intermediate degeneracy ($0.1 < \Theta < 10$), and classical behavior ($\Theta > 10$). The constant ζ lines denote the regions of weak coupling ($\zeta < 0.1$), intermediate coupling ($0.1 < \zeta < 10$), and strong coupling ($\zeta > 10$). The line $\zeta = 119$ is also plotted as a possible freezing curve of the OCP. The dotted line denotes the border of the relativistic domain. Key: *M*1, metallic electrons below room temperature; *M*2, liquid metals expanded to near their critical point; *M*3, shocked aluminum; EHL, electron plasmas in the electron-hole liquids in silicon and germanium; *W*, electrons in white dwarfs; IFE, electrons in inertial fusion plasmas (lower domain is experiment, upper domain is goal); SCN and SCE, nuclei and electrons in solar core; TN and TE, nuclei and electrons in Tokamak plasmas.

hydrogen or tritium nuclei in fusion plasmas, most applications of this work will be found in electron plasmas, and thus we shall in what follows generally use the term "electron liquid" interchangeably with the more general appellation "one-component Fermi plasma."

The OCP is a system consisting of a single species of charged point particles together with a uniform oppositely charged background to ensure charge neutrality. Although the OCP is a theoretical construct on its own, it is nonetheless an essential part of the solution to many important physical problems. For example, by coupling the standard adiabatic (Born-Oppenheimer) approximation with an assumption of a weak electron-ion pseudopotential interaction, it can be shown[3] that the thermodynamics of a simple metal is the sum of that due to a one-component electron plasma and that due to a system of classical ions interacting via a state-dependent pair potential. Furthermore, within the local density approximation of the density functional theory of electronic structure, the excess chemical potential of a one-component electron plasma plays the role of an exchange-correlation potential in the one-electron Schrödinger equation. Finally, the classical OCP is a standard approximation for both astrophysical and laboratory fusion plasmas, where the electrons are now treated as a polarizable background for the ions. It is thus not surprising that there has been a large amount of work carried out on both the zero-temperature fermion OCP (degenerate electron liquid) and the classical OCP.[4–6] At zero temperature, diagrammatic[7] and integral equation[8,9] methods together with recent Monte Carlo calculations[10] have combined to present an accurate description of the paramagnetic electron liquid. Similar methods[11–14] have also led to a precise description of the classical OCP. As mentioned above, however, the problem of the OCP at intermediate degeneracy has only recently received attention, and this paper is addressed in part to the issue of filling in this gap.

The basic criterion that determines the relevance of quantum effects in a plasma is the ratio of the thermal de Broglie wavelength $\lambda_T=(2\pi\hbar^2/mk_BT)^{1/2}$ to the interparticle spacing $d=2a$, where a (the Wigner-Seitz radius or ion-sphere radius) is defined by $4\pi a^3/3=1/n$, with n being the number density. Thus $\lambda_T \gg d$ defines the regime of complete degeneracy, while $\lambda_T \ll d$ defines a nondegenerate regime where quantum effects are negligible and classical statistical mechanics may be used. Throughout this work we will frequently use another parameter to characterize the degree of degeneracy. This is the dimensionless temperature $\Theta=k_BT/\varepsilon_F$, where $\varepsilon_F=\hbar^2k_F^2/2m$ is the Fermi energy of the noninteracting plasma and $k_F=(3\pi^2n)^{1/3}$ is the Fermi wave vector. From the equation

$$\frac{\lambda_T}{d}=\left[\frac{2\alpha^2}{\Theta}\right]^{1/2}=\frac{0.9235}{\sqrt{\Theta}}, \tag{1.1}$$

where $\alpha=(4/9\pi)^{1/3}$, it is seen that the requirement of small (or large) Θ for degenerate (or classical) behavior is essentially the same as the requirement of large (or small) λ_T/d. In this work we find that $\Theta<0.1$ approximately defines the degenerate regime (where the zero-temperature results are quite accurate), while $\Theta>10$–100 defines the nondegenerate regime (where the classical results apply). For $0.1<\Theta<10$ however, the plasma is semidegenerate and inadequately described by either the zero-temperature or classical formalisms.

There are, in fact, many physical systems whose electrons exist in semidegenerate states. For example, the finite-temperature thermodynamic and dielectric properties of the electron liquid are needed for a proper treatment of the equation of state of high-temperature liquid metals found in shock-wave experiments[1] and experiments on liquid metals expanded to near their critical points,[15] of high-density inertially-confined fusion plasmas, and of the finite-temperature exchange-correlation potentials used in density functional calculations of atomic properties at high pressure and temperature.[16] Semidegenerate electron liquids are also found in semiconductors, where the low densities involved lead to correspondingly low Fermi temperatures. For example, Mooradian[17] observed a spectral line in n-type GaAs at $n=1.8\times10^{18}$ cm^{-3} evolve from a form appropriate to a Fermi distribution to that appropriate to a Maxwellian as the temperature was raised from 5 to 300 K. Also, the phase diagram of the electron-hole liquid in irradiated semiconductors spans the regime of semidegeneracy, as is seen from the fact that the critical temperatures in Si and Ge are 23 K and 7 K, respectively, while the electron Fermi energies at the critical densities are 45 K (Si) and 12 K (Ge).[18] The finite-temperature equation of state of the electron liquid is also needed for a quantitative explanation of the miscibility gap in solutions of alkali metals in their alkali-halide metals.[19] In Fig. 1 we have plotted, on a logarithmic temperature-density scale, a wide spectrum of plasmas of physical significance, together with the lines $\Theta=0.1$, 1, and 10, in order that the degree of degeneracy of each plasma may be assessed. Note that the density has been scaled by the effective Bohr radius ($a_0=\hbar^2/me^2$), while the temperature has been scaled by the effective Rydberg (1 Ry$=e^2/2a_0$). (For the ionic plasmas in Fig. 1, these quantities differ from their values for the electronic plasmas by the electron-ion mass ratio.) The significance of the semidegenerate region is apparent.

Previous calculations of the thermodynamic and dielectric properties of the fermion plasma at intermediate degeneracy have been of several types. Pokrant[20] has developed a theory that uses a finite-temperature variational principle to evaluate the diagonal density matrix, which he approximates as a product of an ideal fermion diagonal density matrix and a product of pair functions. He then calculates the energy by using two- and three-body correlation functions obtained from the hypernetted chain and convolution approximations, respectively. However, he presents equation of state data in tabular form only at four densities ($r_s=a/a_0=0.5$, 1, 2, 3.39). Several other groups have studied the thermodynamic[21–25] and dielectric[26,27] properties of the OCP by using finite-temperature perturbation theory within the random-phase approximation. Particularly noteworthy is the work of Perrot and Dharma-wardana[24] and of Kanhere *et al.*,[25] who have recently presented closed-form parametrizations of the exchange-correlation free energy

and chemical potential within the random-phase approximation for the paramagnetic and spin-polarized cases, respectively. The work presented here follows a calculational scheme similar to these approaches. However, it is known that the random-phase approximation (RPA) is a weak coupling theory that results in considerable error at coupling strengths appropriate to metallic densities. Thus, in order to obtain results applicable to more strongly coupled plasmas, we use a dielectric formulation commonly used at zero temperature and in the classical regime that includes static local-field corrections to the RPA. In the following, we use this scheme to study the thermodynamics, the dielectric properties (including plasmon dispersion), and the pair-correlation function of the finite-temperature electron liquid. Calculations of the thermodynamic properties, with local-field corrections included, have also recently been performed independently by Tanaka, Mitake, and Ichimaru.[28] They combine the integral equation scheme of Singwi, Tosi, Land, and Sjölander[8] (STLS) for $\Theta<5$ with the results of calculations using the hypernetted chain approximation in the classical regime to present parametrizations of the excess energy and free energy. As we show below, our calculations of the excess free energy of the intermediate degeneracy regime find good agreement with the more exact results of Tanaka *et al.*

Before doing so, however, it is perhaps worthwhile to delineate the region in the density-temperature diagram of Fig. 1 in which the results of the present calculations are meaningful. To do this we first define $\varepsilon_0(r_s,\Theta)$ as the (purely kinetic) energy per particle of an ideal Fermi gas, with $\varepsilon_0(r_s,\Theta=0)=3\varepsilon_F/5$ and $\varepsilon_0(r_s,\Theta\gg1)=3k_BT/2$ as familiar limiting cases. A reasonable approximation for the relativistic domain in Fig. 1 is the criterion $\varepsilon_0>mc^2$. Thus the current nonrelativistic results are applicable only inside the line $\varepsilon_0=mc^2$, which is drawn in Fig. 1. A further constraint on the applicability of the present calculations can be made by defining a generalized coupling constant ζ as the ratio of a typical potential energy e^2/a to a typical kinetic energy ε_0:

$$\zeta(r_s,\Theta)\equiv\frac{e^2/a}{\varepsilon_0}=\begin{cases}0.905r_s, & \Theta\ll1\\ \frac{2}{3}\Gamma, & \Theta\gg1\end{cases}\tag{1.2}$$

where $\Gamma=e^2/ak_BT$ is the classical coupling constant. As will be shown below through comparison with Monte Carlo results, the present theory gives accurate results for roughly $\zeta<10$. Thus the line $\zeta=10$ is also drawn in Fig. 1, and inside this line the results of the present calculations become increasingly inaccurate (i.e., as ζ increases). Also drawn in Fig. 1 is the line $\zeta=119$, which is the extension through all degeneracies of the classical solid-liquid phase boundary at $\Gamma=178$ as found from the Monte Carlo calculations of Slatterly, Doolen, and DeWitt.[14] Thus the domain $\zeta>119$ is a reasonable estimate of the region of stability of the Wigner crystal. At zero temperature, this corresponds to $r_s>131$, which is of the same order of magnitude as many other estimates for Wigner crystallization of the degenerate electron liquid.[4,7,10,13] Although the present calculations are not applicable to such strongly coupled plasmas, we point to the interesting fact that there exists a maximum density and temperature for the crystalline OCP (in our approximation, $T_{\max}\approx3.8\times10^{-5}$ Ry, $r_s^{\min}\approx131$). As the density is increased at a constant temperature less than $T_{\max}$, the OCP first freezes, but then melts at yet a higher density because of degeneracy pressure. Finally, we observe that the present calculations are only for the paramagnetic liquid phase. The zero-temperature Monte Carlo results of Ceperley[10] do however predict a stable ferromagnetic phase at densities intermediate between those of the paramagnetic liquid and Wigner crystal. The nature of this magnetic phase boundary at finite temperature is thus far an unexplored question.

In the following section we present a detailed account of our calculational scheme. In Secs. III–V we give the results of our calculations of the thermodynamic, dielectric, and pair-correlation functions, respectively. After concluding in Sec. VI, we present in the Appendix the closed-form-fitting expressions for the thermodynamic and dielectric functions as discussed below.

II. CALCULATIONAL SCHEME

In this section we briefly review our theory of the thermodynamic and dielectric properties of a paramagnetic Fermi liquid at any degeneracy. The present method can basically be characterized as a dielectric formulation of the thermodynamic functions, since as we show below, the primary approximation is to the polarizability of the Fermi liquid in terms of that of ideal fermions. Consider then a system of N fermions in a volume V at temperature T, with density $n=N/V$ and chemical potential μ. As usual, the thermodynamic functions are expressed as a sum of ideal fermion, exchange, and correlation parts, e.g., $F=F_0+F_x+F_c$. The basis of our calculation of the excess free energy is the fact that it is expressible as a coupling constant integration over the potential energy.[29] We perform this coupling constant integration in the canonical ensemble (at fixed N, T, and V), to obtain the excess Helmholtz free energy. Previous calculations within the random-phase approximation[21–25] (RPA) have, however, proceeded in the grand canonical ensemble, where an approximate inversion of $n(\mu,T)$ to obtain $\mu(n,T)$ needs to be performed in order to obtain equation-of-state data. It can be seen however, from the discussion of Perrot and Dharma-wardana,[24] that if this inversion is carried out to the same order in perturbation theory as the calculation of the grand potential itself, the results of the two ensembles are equivalent. In the following we use the canonical ensemble, because of the practical and conceptual simplifications involved in using the density as the basic variable.

Before considering the exchange-correlation free energy, we establish the ideal fermion contribution for the sake of completeness. The ideal fermion energy E_0 and pressure p_0 are

$$E_0(T,V,N)=\tfrac{3}{2}p_0V=2V(2\pi)^{-3}\int d^3k\,\varepsilon_k^0 f_k^0\,,\tag{2.1}$$

where (using units with $\hbar=1$) $\varepsilon_k^0=k^2/2m$, $f_k^0=[1+\exp(\beta\varepsilon_k^0-\eta_0)]^{-1}$, $\beta=1/k_BT$, and $\eta_0(n,T)=\beta\mu_0$ is the ideal fermion activity, defined by

$$I_{1/2}(\eta_0)=\tfrac{2}{3}\Theta^{-3/2}\ . \tag{2.2}$$

Here we have used the commonly used notation for the Fermi integral of order ν:

$$I_\nu(\eta)=\int_0^\infty \frac{x^\nu}{1+e^{x-\eta}}dx\ . \tag{2.3}$$

Using this notation, the ideal fermion energy, free-energy, and bulk modulus can be simply expressed as

$$\varepsilon_0(r_s,\Theta)=\frac{3p_0}{2n}=\frac{3\Theta^{5/2}}{2\alpha^2 r_s^2}I_{3/2}(\eta_0)\ \text{Ry}\ , \tag{2.4}$$

$$f_0(r_s,\Theta)=-\tfrac{2}{3}\varepsilon_0(r_s,\Theta)+\mu_0(r_s,\Theta)\ , \tag{2.5}$$

and

$$\frac{1}{n}B_0(r_s,\Theta)=\frac{4}{3\alpha^2 r_s^2\sqrt{\Theta}I_{-1/2}(\eta_0)}\ \text{Ry}\ . \tag{2.6}$$

Accurate closed-form-fitting expressions for $I_{3/2}(\eta_0)$ and $I_{-1/2}(\eta_0)$ as functions of Θ (for the sake of practicality) are presented in the Appendix, while a parametrized inversion $\eta_0(\Theta)$ of Eq. (2.2) is given by Dharma-wardana and Taylor.[23]

We now consider the exchange contributions to the thermodynamics. The coupling constant expression for the excess free energy is[29]

$$F_{xc}(T,V,N)=\int_0^1 d\lambda\frac{1}{\lambda}\langle\lambda U\rangle_\lambda\ , \tag{2.7}$$

where U is the potential-energy operator and $\langle\cdots\rangle_\lambda$ denotes a canonical ensemble average in a system interacting via a Coulombic potential of $\lambda e^2/r$. In Eq. (2.7) the contribution first order in e^2 is the exchange free energy, $F_x=\langle U\rangle_0$, which from a straightforward application of finite-temperature perturbation theory can be written

$$F_x(T,V,N)=-V(2\pi)^{-6}\int d^3k\int d^3q\, v(\mathbf{k}-\mathbf{q})f_k^0 f_q^0\ , \tag{2.8}$$

where $v(q)=4\pi e^2/q^2$. In terms of the Fermi integrals defined in Eq. (2.3), this can be conveniently expressed as[30]

$$f_x(r_s,\Theta)\equiv\frac{F_x}{N}=\frac{-3\Theta^2}{4\pi\alpha r_s}\int_{-\infty}^{\eta_0(\Theta)}d\eta\, I_{-1/2}^2(\eta)\ \text{Ry}\ . \tag{2.9}$$

Similarly, the exchange parts of the chemical potential and bulk modulus are

$$\mu_x(r_s,\Theta)=\frac{-1}{\pi\alpha r_s}\sqrt{\Theta}I_{-1/2}(\eta_0)\ \text{Ry}\ , \tag{2.10}$$

and

$$\frac{1}{n}B_x(r_s,\Theta)=\frac{-4}{3\pi\alpha r_s\Theta}\frac{I'_{-1/2}(\eta_0)}{I_{-1/2}(\eta_0)}\ \text{Ry}\ . \tag{2.11}$$

The exchange pressure is $p_x/n=\mu_x-f_x$, and because of the $1/r_s$ scaling in Eq. (2.9), the exchange energy can be expressed as $\epsilon_x=3\mu_x/2-f_x$. (Equivalently, this follows from the virial theorem). It is worth noting that all of these quantities vanish as $1/\Theta$ at high temperatures ($\Theta\gg1$). However, even at temperatures as high as $\Theta=1$, ($T=T_F$), the exchange contributions are still comparable to those at $T=0$. Accurate closed form Padé approximants for Eqs. (2.10) and (2.11) are presented in the Appendix, from which small and large Θ expansions can be read off. A closed-form parametrization of $f_x(r_s,\Theta)$ is given by Perrot and Dharma-wardana.[24] We point out, however, that this fit to f_x does not include the weak logarithmic singularity at small Θ:[22]

$$f_x(r_s,\Theta\ll1)=\frac{-3}{2\pi\alpha r_s}\left[1-0.853\Theta^2+\frac{\pi^2}{6}\Theta^2\ln\Theta+\cdots\right]\text{Ry}\ . \tag{2.12}$$

This singularity is, of course, cancelled by a similar term in the correlation free energy.

We now examine the correlation contribution to the thermodynamics. If the exchange part is subtracted from the excess free energy defined by the coupling constant integration of Eq. (2.7), and the potential energy is expressed in terms of the static structure factor $S(q)$, the correlation free energy can be written

$$F_c(T,V,N)=\frac{N}{2}\int_0^1 d\lambda\frac{1}{\lambda}\int\frac{d^3q}{(2\pi)^3}v_\lambda(q)[S_\lambda(q)-S_0(q)]\ . \tag{2.13}$$

Relating the static structure factor to the retarded polarizability $\chi(q,\omega)$ by the fluctuation-dissipation theorem[31]

$$S(q)+N\delta_{q,0}=\frac{-1}{n}\int_{-\infty}^{\infty}\frac{d\omega}{2\pi}\coth\left[\frac{\beta\omega}{2}\right]\text{Im}\chi(q,\omega) \tag{2.14}$$

readily permits (2.13) to be rewritten as

$$F_c=\frac{-V}{2}\int_0^1 d\lambda\frac{1}{\lambda}\int\frac{d^3q}{(2\pi)^3}\int\frac{d\omega}{2\pi}v_\lambda(q)\coth\left[\frac{\beta\omega}{2}\right]\times\text{Im}[\chi_\lambda(q,\omega)-\chi_0(q,\omega)]\ , \tag{2.15}$$

where $\chi_0(q,\omega)$ is the ideal fermion polarizability.

As mentioned previously, the evaluation of (2.15) within the RPA, where $\chi_{\text{RPA}}=\chi_0/(1-v_q\chi_0)$, leads to overly negative correlation energies at metallic densities. This is because the RPA pair-correlation function [obtained by using χ_{RPA} in Eq. (2.14)] is actually quite negative at small distances, which can be attributed to the RPA's erroneous inclusion of the self-field of the electron in determining the dielectric response. In order to include local-field corrections in the pair-correlation function, we follow an approximate procedure commonly used both at zero-temperature[4,32–34] and in the classical regime,[4] where the polarizability is related to its ideal part by

$$\chi(q,\omega)=\frac{\chi_0(q,\omega)}{1-[1-G(q)]v(q)\chi_0(q,\omega)}\equiv\frac{\chi_0(q,\omega)}{\xi(q,\omega)}\ . \tag{2.16}$$

Here $G(q)$ contains the local-field corrections to the RPA ($G=0$ in the RPA).

The relation (2.16) is our fundamental approximation in calculating the dielectric and thermodynamic properties of the semidegenerate OCP. It has in the past been motivated by several different routes. Hubbard[32] first used the approximation (2.16) in his calculation of the electron gas ground-state energy. He showed how such a form followed from an approximate evaluation of the higher-order "exchange-conjugate" diagrams to the "bubble" diagrams of the RPA polarizability. Langreth[35] and Vignale and Singwi[36] have shown how the form (2.16) follows from approximating the effective particle-hole interaction $\tilde{I}$ by a static form dependent only on the momentum transfer along the particle-hole channel (a "local" approximation):

$$\tilde{I}_{q\omega}(\mathbf{k}_1,\omega_1;\mathbf{k}_2,\omega_2)\rightarrow\tilde{I}(q)=-2v(q)G(q)\ . \tag{2.17}$$

Finally, the polarization potential approach of Pines[37] allows for a more physical derivation of Eq. (2.16) by introducing $v(q)[1-G(q)]\langle\rho(q,\omega)\rangle$ as the pseudopotential with which electrons couple to induced density fluctuations $\langle\rho(q,\omega)\rangle$. The relation (2.16) is then immediately obtained by assuming that electrons respond as independent particles [i.e., via $\chi_0(q,\omega)$] to the sum of the external field and the *modified* polarization field[4,34]

$$\begin{aligned}\phi_{\rm pot}(q,\omega)&=[1-G(q)]\phi^0_{\rm pol}(q,\omega)\\&=v(q)[1-G(q)]\langle\rho(q,\omega)\rangle\ .\end{aligned} \tag{2.18}$$

From this it is seen that $[1-G(q)]$ partially corrects for the RPA assumption of independent particle response to $\phi_{\rm ext}+\phi^0_{\rm pol}$: since $G(q)\geq 0$, the factor $[1-G(q)]$ weakens the coupling to the polarization field and thus approximately accounts for the neglect of short-range correlations inherent in the use of the independent particle response function. We stress however, that the assumption of a static LFC function is only a convenient approximation, which (as discussed in Sec. IV following) neglects some of the dynamical and dissipative aspects of the true local field.

In order to determine $G(q)$, we make use of the two standard constraints upon it. First, the compressibility sum rule[38] requires that $G(q\rightarrow 0)=\gamma(q/2k_F)^2$, where the parameter γ is related to the excess bulk modulus

$$\gamma(r_s,\Theta)=\frac{-3\pi\alpha r_s}{2}\frac{B_{xc}(r_s,\Theta)}{n\ \mathrm{Ry}}\equiv\gamma_x(\Theta)+\gamma_c(r_s,\Theta)\ . \tag{2.19}$$

Secondly, the cusp condition on short range correlations[39] requires that $G(q\rightarrow\infty)=1-g(0)$, where $g(0)$ is the pair-correlation function at $r=0$. These two constraints are conveniently included in $G(q)$ by use of the Vashista-Singwi form[9] for the local-field-correlation (LFC) function

$$G(q)=A(1-e^{-Bq^2})\ , \tag{2.20}$$

where A and B are determined by $\gamma(r_s,\Theta)$ and $g(0)$. Here we have simply fixed $g(0)$ to a value appropriate for metallic densities,[4] i.e., $g(0)=0.1$, because the large q behavior of $\chi(q,\omega)$ is rather insensitive to $G(q)$ [note that $v(q)\chi_0(q,\omega)$ which multiplies $G(q)$ in the denominator of (2.16) vanishes as q^{-4} at large q]. The function $\gamma_x(\Theta)$ is then calculated from a closed-form parametrization of Eq. (2.11) which is presented in the Appendix, while $\gamma_c(r_s,\Theta)$ is obtained from an appropriate interpolation between known Monte Carlo results at zero temperature[40] and in the classical regime.[13] We note that the error at intermediate degeneracy caused by this *ad hoc* interpolation is a second-order effect, since we have found that the final F_c calculated is quite insensitive to the form of interpolation. At temperatures where $\Theta<1$ this is to be expected because γ_x strongly dominates γ_c. Further evidence for this is the fact that Hubbard[32] obtained quite good results for the zero-temperature electron gas correlation energy, even though his value of γ was in error by a factor of 2. The present scheme for the determination of local-field correlations thus hinges solely on the determination of a correlation length $r_\gamma\approx a\sqrt{\gamma}$, within which short-range correlations, not included in the RPA are approximately accounted for.

In Fig. 2 the results of the present calculation of the static LFC function $G(q)$ are compared with other calculations, in both zero-temperature and classical regimes. At zero temperature (and $r_s=2$) we make comparison to the following: (a) Utsumi and Ichimaru[41] who have used an equation of motion approach for the Wigner distribution to obtain $G(q)$; (b) Iwamoto, Krotscheck, and Pines[34] who have obtained $G(q)$ from existing Monte Carlo calculations of $S(q)$ by assuming the spectral function $\mathrm{Im}\chi(q,\omega)$ to consist of a single delta-function peak only; (c) Vashista and Singwi[9] who have modified the self-consistent integral equation theory of Singwi *et al.*[8] for $G(q)$ by partially including three-body correlations in order that the compressibility sum rule be satisfied; (d) Iwamoto and Pines[34] who have obtained the LFC function by combining existing Monte Carlo calculations of the compressibility and spin susceptibility with a theory

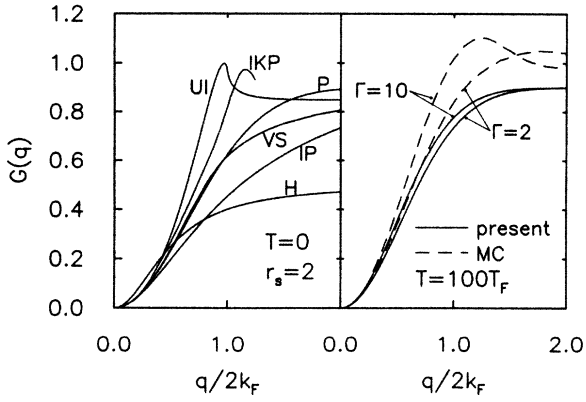

FIG. 2. Static LFC function $G(q)$ in various theories at $T=0$ and in the classical regime ($\Theta=100$). Notation is UI, Utsumi and Ichimaru (Ref. 38); IKP, Iwamoto, Krotscheck, and Pines (Ref. 34); *P*, present; VS, Vashishta and Singwi (Ref. 9); IP, Iwamoto and Pines (Ref. 34), *H*, Hubbard (Ref. 32). The dashed lines labeled MC on the right are the Monte Carlo based curves of Tago, Utsumi, and Ichimaru (Ref. 42).

that accounts for both the spin symmetric and spin antisymmetric components of $G(q)$; and (e) finally, as mentioned previously, Hubbard[32] who used an approximate evaluation of higher-order polarization diagrams to calculate $G(q)$. In the classical regime, comparison is made to the LFC functions obtained by Tago, Utsumi, and Ichimaru[42] from existing Monte Carlo calculations of $S(q)$. In both cases, it is seen that although the form (2.20) misses the peaked structure at $q \approx 2k_F$ predicted in some of the theories, it is nonetheless a very reasonable approximation for the LFC function in general.

Having thus detailed our calculation of the OCP polarizability, we now return to the calculation of the correlation free energy as given in Eq. (2.15). In order to proceed with the evaluation of F_c, one further approximation is made. Specifically, the coupling constant integration of Eq. (2.15) can be carried out in closed form if the λ dependence of $G(q)$ is neglected. Since γ_x is independent of e^2, this is a very good approximation for $\Theta < 1$. (Iwamoto, Krotscheck, and Pines[34] point out that it leads to errors of less than 1% at zero temperature.) With this approximation, we obtain

$$F_c = \frac{V}{2}\int \frac{d^3q}{(2\pi)^3}\int \frac{d\omega}{2\pi}\coth\left[\frac{\beta\omega}{2}\right] \times[1-G(q)]^{-1}[\arg(\xi)-\mathrm{Im}(\xi)]\,, \tag{2.21}$$

where $\xi(q,\omega)$ is defined in Eq. (2.16) and $\arg(z)$ is the argument of the complex number z. This form for F_c is essentially a finite-temperature generalization of the zero-temperature form of Hubbard[32] but with an improved $G(q)$ (i.e., one that satisfies the compressibility sum rule and also has more correct behavior at large q). Equation (2.21) is evaluated numerically in order to obtain the correlation free energy; note that it requires a three-dimensional numerical integration. A closed form parametrization of $f_c(r_s,\Theta) \equiv F_c/N$, valid for all Θ and for r_s between 1 and 6, is presented in the Appendix. In the subsequent sections, we describe the results of the calculations of the thermodynamic, dielectric, and pair-correlation functions of the OCP.

III. EXCHANGE-CORRELATION THERMODYNAMICS

In this section we present our results for the calculation of the thermodynamic functions of the electron gas at any degeneracy. Through comparison with other recent work on the degenerate electron liquid and classical OCP, we are able to gauge the range of validity of the present calculational scheme. Comparison is also made at intermediate degeneracy to the previous RPA calculations,[24] and also those of Pokrant[20] and Tanaka, Mitake and Ichimaru.[28]

We begin by plotting in Fig. 3 the exchange contributions to the thermodynamic functions versus Θ, at $r_s = 1$. Note, however, that all five functions plotted scale as $f(\Theta)/r_s$, where $f(\Theta)$ is a function of Θ alone. It thus follows that values at any density can also be extracted from this plot. All the curves were obtained from the fitting procedure described previously and in the Appendix. Note that several of the functions have a peaked structure near $\Theta = 1$, and that they all vanish as $1/\Theta$ for $\Theta \gg 1$. It is observed in Fig. 3, however, that the exchange thermodynamic functions do not become small compared to their $T = 0$ values until $\Theta > 10$ or so.

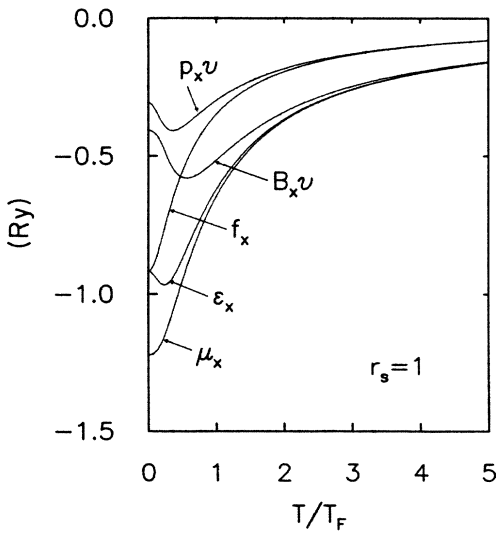

FIG. 3. Exchange contributions to the thermodynamics at $r_s = 1$ as a function of $\Theta = T/T_F$. Here $v = 1/n$. Note that all five functions plotted scale as $1/r_s$ times a function of Θ, so that their value at any r_s can also be obtained.

Consider now the correlation contribution to the free energy. In Fig. 4 we compare our calculated values of the zero-temperature correlation energy to the RPA values,[40] to those of the variational theory of Pokrant[20] described in Sec. I, to Vosko, Wilk, and Nusair's fit[40] to the Monte Carlo values of Ceperley and Alder,[10] to the self-consistent STLS calculations of Tanaka *et al.*[28] and to the

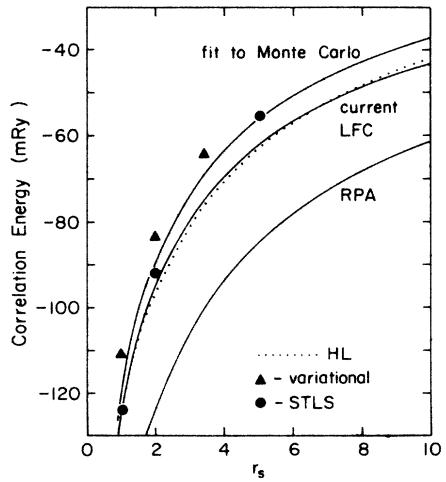

FIG. 4. Comparison of various calculations of the zero-temperature correlation energy. Fit to Monte Carlo and RPA are from Vosko *et al.* (Ref. 40) current LFC is the present theory, the dotted line marked HL is the interpolation form of Hedin and Lundqvist (Ref. 43), while the solid triangles are the results of Pokrant (Ref. 20), and the solid circles are from Tanaka *et al.* (Ref. 28).

commonly used interpolation form of Hedin and Lundqvist.[43] The overestimation of the correlation energy by the RPA is quite apparent and is fairly well corrected in all the other theories. For example, at $r_s=2$, the RPA value of ϵ_c differs by 37% from the Monte Carlo result, while the STLS, present, and variational theories differ by 2%, 5%, and 7%, respectively. It is interesting that the results of the present calculation coincide very nearly with the Hedin-Lundqvist interpolation form. By fixing $G(q)=0$ in our evaluation of Eq. (2.21), we were able to reproduce the RPA values of Vosko *et al.*[40] with deviations less than 1%; this served as a convenient check on the accuracy of our numerics.

Similar behavior is found in the classical regime, as can be seen in Fig. 5 where the results of the present calculation of the excess free energy are compared to the Monte Carlo results of Hansen,[13] to the hypernetted-chain (HNC) calculations of Tanaka *et al.*,[28] and to the RPA results. Classically these RPA results are equivalent to those from Debye-Hückel theory, where

$$\frac{F_{\text{excess}}^{\text{DH}}}{Nk_BT}=\frac{-1}{\sqrt{3}}\Gamma^{3/2}. \tag{3.1}$$

Again, is it seen that inclusion of local-field corrections according to Eq. (2.16) has largely corrected for the overestimate of the correlation energy found in the RPA. We note, however, that at coupling strengths beyond $\Gamma\approx 10$ the present calculations also lead to substantial errors. This is the basis of our earlier remark that the present calculations are accurate only at coupling strengths less than about 10. As is seen in Fig. 1, however, this seems to include most of the important physical plasmas. Figures 4 and 5 also show that the STLS and HNC calculations of Tanaka *et al.* do reproduce the Monte Carlo results more accurately than the present LFC approximation. However, the present approximation, being calculationally more tractable [our form for $G(q)$ is essentially the first iteration in the self-consistent STLS scheme], allows us to analyze quantities such as the pair-correlation function which are computationally more demanding.

It is perhaps worth pointing out how the classical limit is obtained from our quantum formulation of Eq. (2.21). By evaluating the RPA ($G=0$) counterpart of Eq. (2.21) with Boltzmann statistics, DeWitt[44] has shown that the diffraction type quantum corrections to the RPA excess free energy are given by

$$F_{\text{excess}}^{\text{RPA}}=F_{\text{excess}}^{\text{DH}}\left[1-0.424\left(\frac{\Gamma}{\Theta}\right)^{1/2}+0.204\left(\frac{\Gamma}{\Theta}\right)-0.182\left(\frac{\Gamma}{\Theta}\right)^{3/2}+\cdots\right], \tag{3.2}$$

where the classical Debye-Hückel result is given in Eq. (3.1). Thus, within the RPA, the classical limit is obtained at increasingly larger Θ as Γ is increased. Such behavior was in fact observed in our numerical evaluation of the RPA curve in Fig. 5. Within the present LFC theory, however, no such behavior is definitely observed, and, with Γ kept constant, the excess free energy actually becomes independent of Θ for $\Theta>100$ or so. The LFC curve in Fig. 5 is obtained therefore with Θ fixed at 171 ($\eta_0=-8.0$).

In Fig. 6 we compare the results of the present calculation of the correlation free energy at intermediate degeneracy, to those of the variational,[20] RPA,[24] and STLS[28] theories. The present LFC curve is obtained by using the closed-form parametrization of $f_c(r_s,\Theta)$ given in the Appendix. Note that the RPA overestimate of the correla-

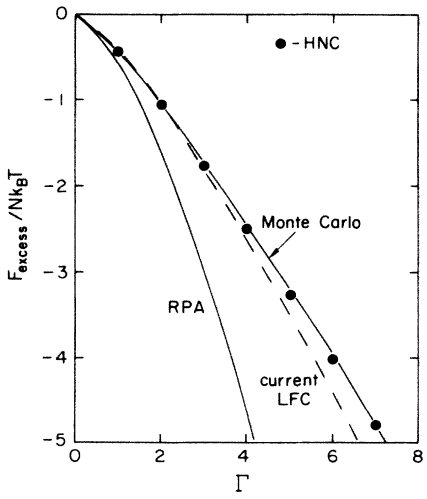

FIG. 5. Excess free energy in the classical regime, versus the classical coupling constant $\Gamma=e^2/ak_BT$. Current LFC is the present theory. The Monte Carlo results are from Hansen (Ref. 13), and the hypernetted chain (HNC) results are from Tanaka *et al.* (Ref. 28).

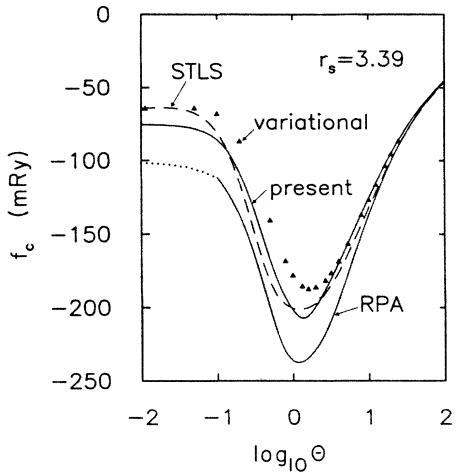

FIG. 6. Correlation free energy at $r_s=3.39$ throughout the degenerate to classical regime. The variational results are from Pokrant (Ref. 20), and the STLS results are from Tanaka *et al.* (Ref. 28). The solid RPA line is from the parametrization of Perrot and Dharma-wardana (Ref. 24), which is valid only at $\Theta>0.1$; the curve is thus interpolated via the dotted line to the zero-temperature RPA value.

tion energy, attributable to its overaccounting for the exchange-correlation hole, does indeed extend throughout the region of intermediate degeneracy. As with the zero-temperature results, the variational theory of Pokrant gives slightly smaller (in magnitude) free energies than the present or STLS theories. Note that all the curves approach the RPA result at large Θ. This happens because as the temperature is increased at fixed density, the coupling constant ζ decreases, so that $\zeta=2\Gamma/3\ll 1$ in the classical regime of Fig. 6, and the RPA theory is accurate.

Given the rather good comparison between the various calculations of the correlation free energy as seen in Fig. 6, it is reasonable to assume that the fitting expressions given here (in the Appendix) and by Tanaka *et al.*[28] both represent a very accurate description of the semidegenerate electron liquid thermodynamics. In particular, the pronounced minimum in the correlation free energy f_c at $\Theta\approx 1$ must be a realistic effect. (Note that this implies that the correlation entropy is positive at low temperatures, but negative at high temperatures.) We point out, however, that when the exchange contribution f_x (see Fig. 3) is added to f_c this minimum is no longer seen, and the excess free energy f_{xc} actually remains fairly constant for temperatures less than T_F at fixed density. This simply reflects the fact that the coupling constant $\zeta(r_s,\Theta)$ remains quite constant under these circumstances [see Eqs. (1.2), (2.4), and (A3)].

The significance of the parameter $\zeta(r_s,\Theta)$ as a coupling constant is clearly depicted in Fig. 7, where f_{xc} and f_c are plotted as a function of Θ at fixed values of ζ. Note that for $\Theta<0.1$, the ground-state values are obtained, while for $\Theta>10$–100, f_x vanishes and f_{xc} takes on its constant classical value. Note also that plasmas within nearly two decades of coupling strength all have excess free energies of order $-e^2/a$, for all temperatures. This scaling of f_{xc} by e^2/a is not complete however, for although $f_{xc}(\Theta=0)/(e^2/a)$ is fairly constant throughout the full

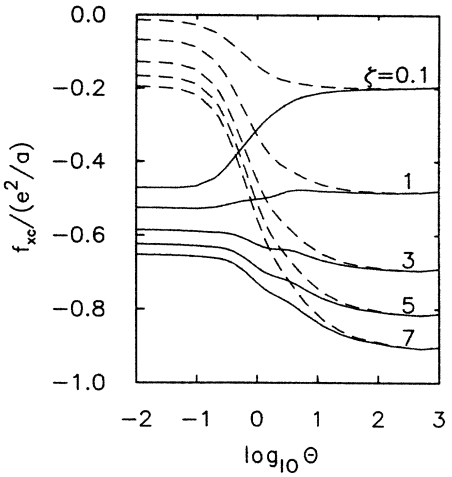

FIG. 7. Exchange-correlation (solid curves) and correlation only (dashed curves) free energy throughout the degenerate to classical regime at fixed values of the coupling constant ζ. Note that the small oscillations in f_{xc} at intermediate degeneracy stem from the approximate nature of our definition of the coupling constant ζ [see Eq. (1.2)].

range of paramagnetic densities, and although $f_{xc}(\Theta\gg 1)/(e^2/a)$ approaches a constant for Γ (or $\zeta)\gg 1$,[14] the same classical ratio vanishes like $\sqrt{\Gamma}$ as $\Gamma\to 0$ due to the e^3 behavior of the Debye-Hückel free energy [see Eq. (3.1)]. This behavior is seen clearly in Fig. 7.

IV. DIELECTRIC PROPERTIES

In this section we study the implications of Eq. (2.16) for the polarizability $\chi(q,\omega)$ and for the dielectric function, energy-loss function, and plasmon dispersion. Our interest is in both obtaining a qualitative understanding of how the dielectric function evolves from its degenerate to classical form,[26,27] and in presenting a quantitative theory that leads to a very practical closed form description of the dielectric function $\epsilon(q,\omega)$ at any density and temperature.

The dielectric function is related to the polarizability by

$$\epsilon^{-1}(q,\omega)=1+v(q)\chi(q,\omega)\ , \tag{4.1}$$

or equivalently,

$$\epsilon(q,\omega)=1-v(q)\chi_{sc}(q,\omega)\ , \tag{4.2}$$

where $\chi_{sc}(q,\omega)=\epsilon(q,\omega)\chi(q,\omega)$ is the irreducible polarizability, which measures the electronic response to *screened* external fields. Within our "extended-RPA" theory of Eq. (2.16), the irreducible polarizability is given by

$$\chi_{sc}(q,\omega)=\frac{\chi_0(q,\omega)}{1+v(q)G(q)\chi_0(q,\omega)}\ , \tag{4.3}$$

where the LFC function $G(q)$ is discussed fully in Sec. II. The ideal fermion retarded polarizability is given by[45]

$$\chi_0(q,\omega)=-2\int\frac{d^3p}{(2\pi)^3}\frac{f^0_{\mathbf{p}+\mathbf{q}}-f^0_{\mathbf{p}}}{\omega+i\delta-(\varepsilon^0_{\mathbf{p}+\mathbf{q}}-\varepsilon^0_{\mathbf{p}})}\ , \tag{4.4}$$

where δ is a positive infinitesimal. If a dimensionless response function $F^0(q,\omega)$ is defined by $F^0_1+iF^0_2=v(q)\chi_0(q,\omega)$, the imaginary part of $\chi_0(q,\omega)$ can be evaluated from Eq. (4.4) to be[27]

$$F^0_2(Q,z)=\frac{-\alpha r_s\Theta}{8Q^3}\ln\left\{\frac{1+\exp\left[\eta_0-\frac{1}{\Theta}\left[\frac{z}{Q}-Q\right]^2\right]}{1+\exp\left[\eta_0-\frac{1}{\Theta}\left[\frac{z}{Q}+Q\right]^2\right]}\right\}\ . \tag{4.5}$$

Here we define scaled momentum and frequency variables by $Q=q/2k_F$ and $z=\omega/4\varepsilon_F$. Similarly, the real part of $\chi_0(q,\omega)$ can be expressed as[27]

$$F^0_1(Q,z)=\frac{\alpha r_s}{4\pi Q^3}\left[\phi\left[\frac{z}{Q}+Q\right]-\phi\left[\frac{z}{Q}-Q\right]\right]\ , \tag{4.6}$$

where

$$\phi(x)=\int_0^\infty dy\frac{y}{1+\exp\left[\frac{y^2}{\Theta}-\eta_0\right]}\ln\left|\frac{x-y}{x+y}\right|\ . \tag{4.7}$$

For many purposes it is convenient to have a closed-form expression for $F_1^0(Q,z)$. For this reason, we have generalized the zero-temperature Padé approximate form of Pettifor and Ward[46] for $F_1^0(Q,z=0)$ to nonzero temperatures and nonzero frequencies. This extension is made possible for two reasons. First, the r_s dependence of $F_1^0(Q,z;r_s,\Theta)$ scales out, as seen in Eq. (4.6). Second, the Q and z dependence of F_1^0 is folded into a single variable $x=z/Q\pm Q$. Thus it is only necessary to parametrize $\phi(x;\Theta)$ in order to describe F_1^0 completely. This is accomplished by writing

$$\phi(x;\Theta)=\sqrt{\Theta}I_{-1/2}(\eta_0)x\tilde{\phi}(x;\Theta) \tag{4.8a}$$

and

$$\tilde{\phi}(x;\Theta)=\frac{1+\sum_{j=1}^{4}a_{2j}(\Theta)x^{2j}}{1+\sum_{j=1}^{5}b_{2j}(\Theta)x^{2j}} . \tag{4.8b}$$

Here $I_{-1/2}(\eta_0)$ is the Fermi integral defined in Eq. (2.3). The functions $b_j(\Theta)$ are determined by considering the small and large x behavior of $\phi(x)$, while the functions $a_j(\Theta)$ are then obtained by fitting the form (4.8) to the exact $\phi(x)$ in Eq. (4.7). This procedure is detailed in the Appendix. The form (4.8) is indeed quite useful. For example, in our preliminary discussion of this work[1] we have shown that (4.8) leads to a closed-form expression for the state-dependent pair potentials in simple metals which emerges as the sum of complex Yukawa potentials. Also, when (4.8) is used rather than (4.7) in the numerical evaluation of F_c in Eq. (2.27), results that differ by at most 2% are obtained, but in 2 orders of magnitude less computing time. In the remainder of this section we use Eqs. (4.2)—(4.6) and (4.8) to make some general observations concerning the dielectric properties of the OCP throughout the full range of electron degeneracy.

The most obvious effect of an increasing temperature on the dielectric function is a broadening of its peaked structure, due, of course, to the evolution of the Fermi distribution function from a sharp step function to a broad Maxwellian. An immediate consequence of this is that exponential tails develop in the region (at zero temperature) of forbidden single particle-hole excitations: where $z>Q^2+Q$ or $z<Q^2-Q$. These features are clearly seen in the contour plots of $\mathrm{Re}\epsilon(q,\omega)$ and $\mathrm{Im}\epsilon(q,\omega)$ shown in Fig. 8 at the three temperatures $\Theta=0.01$, 1, and 10 (with $r_s=4$). Note, for example, how the contour $\mathrm{Im}(\epsilon)=0.01$ evolves from the line $z=Q^2+Q$ at $\Theta=0.01$, to regions of larger energy absorption for a given change in momentum. Note also how the nonanalytic structure in $\epsilon(q,\omega)$ at $z=Q-Q^2$ and $\Theta=0.01$, due to the sharp Fermi surface, is washed out at higher temperatures. Furthermore, note that the *magnitude* of the peaked structure in $\epsilon(q,\omega)$ near its singularity at the origin decreases with increasing temperature, as it must due to sum rule constraints. Inspection of the $\mathrm{Re}(\epsilon)=0$ contours in the top panels of Fig. 8 shows how the small q plasmon dispersion increases with temperature. Also, comparison of these plasmon curves with the corresponding regions where $\mathrm{Im}\epsilon(q,\omega)$ becomes non-negligible demonstrates

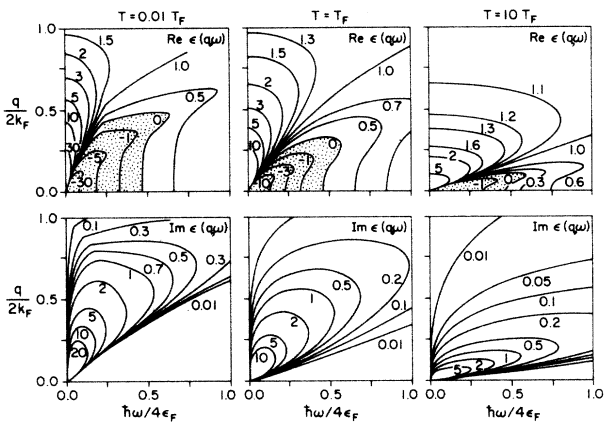

FIG. 8. Contour plots of the real and imaginary parts of $\epsilon(q,\omega)$ at $\Theta=0.01$, 1, and 10 and $r_s=4$. The curves were obtained by using the approximation (4.8) for $\mathrm{Re}\chi_0(q,\omega)$, together with the static LFC approximation of Eq. (4.3).

quantitatively how the Landau damping of the plasmon begins at smaller wave vectors as the temperature is increased. These features can similarly be seen in Fig. 9, where the energy-loss function

$$\mathrm{Im}\left[\frac{-1}{\epsilon(q,\omega)}\right]=-v(q)\mathrm{Im}\chi(q,\omega)$$
$$=v(q)\tanh\left[\frac{\beta\omega}{2}\right]S(q,\omega) \tag{4.9}$$

is plotted at the same density and the same three tempera-

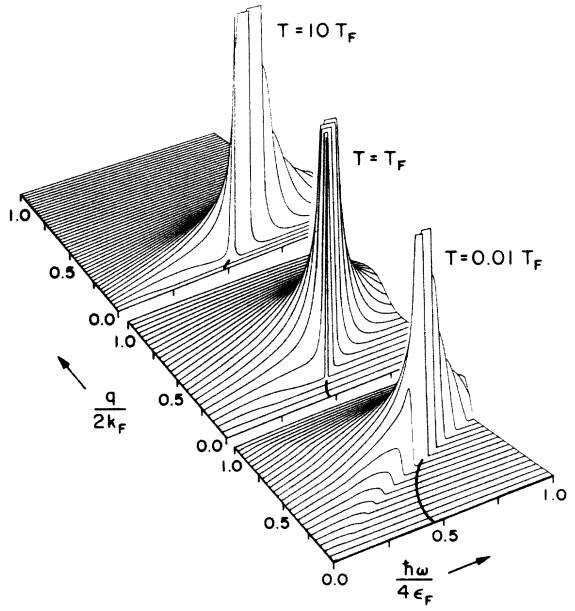

FIG. 9. Energy-loss function $\mathrm{Im}[-1/\epsilon(q,\omega)]$ at $r_s=4$ and $\Theta=0.01$, 1, and 10. The bold solid lines denote the position of the delta-function peak of the undamped plasmon. Note that all the curves are truncated at $\mathrm{Im}[-1/\epsilon(q,\omega)]=3$.

tures. Here the bold solid lines represent the delta-function-like peaks of the nearly undamped plasmons at $\omega_p(q)$. It is apparent that this undamped plasmon broadens once it enters the area of Landau damping where $\mathrm{Im}\epsilon(q,\omega)$ is non-neglible. The increasing dispersion with temperature of the peak in the energy-loss function is also seen in Fig. 9. Also noteworthy is the double-peaked structure in $S(q,\omega)$ at low temperatures, near where the plasmon $\omega_p(q)$ enters the boundary of the particle-hole continuum $z=Q^2+Q$. (See, for example, the $Q\approx 0.45$ curves in the low-temperature plot of Fig. 9.) In general, the evolution of the dielectric function from its low- to high-temperature form reflects a decrease in the screening capabilities of the electron liquid. This is quite apparent in Figs. 8 and 9, where the energy and wave-vector scales are seen to progress from scales based on the Fermi energy and Thomas-Fermi wave vector at low temperatures, to ones based on the temperature and Debye-Hückel screening vector at high temperatures.

With these qualitative features of temperature effects on the plasmon dispersion in mind, we now present a quantitative description of this problem. Following the RPA work of Arista and Brandt,[27] it is straightforward to show that the small q plasmon dispersion described by the LFC form for $\chi(q,\omega)$ is given by

$$\omega_p^2(q)=\omega_{p0}^2[1+A_2(r_s,\Theta)Q^2+A_4(r_s,\Theta)Q^4+\cdots]\ . \tag{4.10}$$

Here $\omega_{p0}^2=4\pi ne^2/m$ and

$$A_2(r_s,\Theta)=\frac{9\pi}{2\alpha r_s}\Theta^{5/2}I_{3/2}(\eta_0)-\gamma(r_s,\Theta)\ , \tag{4.11}$$

$$A_4(r_s,\Theta)=\frac{9\pi^2}{\alpha^2 r_s^2}\left[\tfrac{3}{2}\Theta^{7/2}I_{5/2}(\eta_0)-\tfrac{9}{4}\Theta^5 I_{3/2}^2(\eta_0)\right]+\frac{3\pi}{\alpha r_s}-\tilde{\gamma}(r_s,\Theta)\ , \tag{4.12}$$

and γ and $\tilde{\gamma}$ are defined by $G(q\to 0)=\gamma Q^2+\tilde{\gamma}Q^4$. The fact that γ, related in Eq. (2.19) to the excess bulk modulus by the compressibility sum rule, is generally positive means that the inclusion of static local-field corrections decreases the plasmon dispersion at small q. This is an important feature, since the experimentally obtained values of A_2 for Be, Mg, Li, Ba, Na, and K are all between 0.4 and 0.9 of the RPA predictions A_2^{RPA} [given by (4.11) with $\gamma=0$].[4] Both these effects of temperature and local-field corrections are shown clearly in Fig. 10, where the plasmon dispersion, defined by

$$\omega_p(q)=\max_{\omega}\{\mathrm{Im}[-1/\epsilon(q,\omega)]\}\ , \tag{4.13}$$

is plotted at $r_s=2$ and $\Theta=0.01$, 1, and 10. For the low-temperature case, comparison is also made to the experimental data of Batson, Chen, and Silcox[47] on the nearly free electron metal aluminum, and to the dynamical LFC theory of Holas, Aravind, and Singwi.[48] Note that although the present LFC theory does lead to some improvement on the agreement with the experimental data at $q\approx 1.5k_F$, it still leaves a large disparity near $q\approx k_F$. (These wave vectors are sufficiently large that band-structure effects should not be significant here.[49]) By comparison, the theory of Holas *et al.*, which by way of a dynamical (and complex) LFC function $G(q,\omega)$ includes dissipative effects of the local field, finds much better agreement with the data on aluminum.

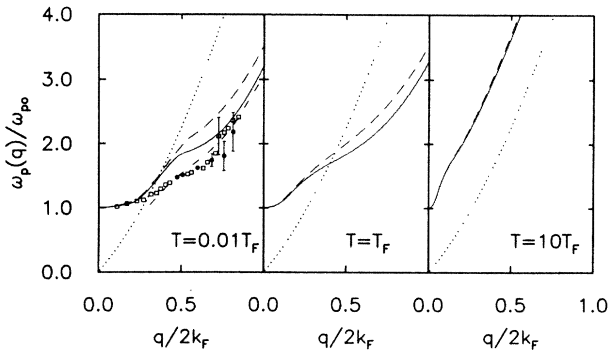

FIG. 10. Plasmon dispersion (defined by the peak position of the energy-loss function) at $r_s=2$ and $\Theta=0.01$, 1, and 10. Solid curve is present theory, dashed curve is RPA, and the dotted curve is the border of the zero-temperature particle-hole continuum. At $\Theta=0.01$, the dot-dashed curve is from the dynamical LFC theory of Holas *et al.* (Ref. 48), while the experimental points are those of Batson *et al.* (Ref. 47) for aluminum.

Given the state of comparison between the present theory and experiment, as shown in Fig. 10, it is perhaps worthwhile to present a more detailed assessment of the validity of our fundamental assumption given by Eq. (2.16) [or equivalently, Eq. (4.3)]. In general, of course, the LFC function will be dynamical and complex. The present assumption of a static LFC function implies that the exchange-correlation hole moves rigidly with the electron. This should be a reasonable approximation so long as the frequencies of the external fields to which we are seeking the electronic response to are much less than the plasma frequency.[48] Correspondingly, our assumption that the LFC function is entirely real implies a neglect of the dissipative aspects of the spin and Coulomb correlations that determine the true dynamical local field. The present extended-RPA theory also considers only the collective plasmon branch and single particle-hole excitations in the spectral function; it neglects the contributions due to multipair excitations. [Note, for example, that within the present theory at $T=0$, $\mathrm{Im}\chi(q,\omega)$ vanishes exactly where $\mathrm{Im}\chi_0(q,\omega)$ does, which is just the forbidden region of *single* particle-hole excitations.] Iwamoto *et al.*[34] point out that although the f sum rule is satisfied by the static approximation (2.16), the compressibility sum rule and ω^3 sum rule cannot both be satisfied. Finally, we note that the neglect of multipair excitations means that we were not able to obtain the high-frequency tail (at $z>Q^2+Q$) in the experimental measurements of the energy-loss function in the degenerate electron liquid.[48] This has also been suggested as the cause of the failure of static LFC theories to explain the double-peaked structure of $S(q,\omega)$ found in some metals, such as beryllium at $Q=0.73$ and 0.88.[34] These shortcomings of the present dielectric formulation are shared, at least in part, by all first-principle theories

espoused to date. (As mentioned above, however, attempts have been made to include dynamical effects, and to satisfy the various sum rules.)

In Figs. 11 and 12 we compare $\epsilon(q,\omega)$ and $\mathrm{Im}[-1/\epsilon(q,\omega)]$ (at $q=k_F$, $r_s=2$, and $T=0$) as calculated within the RPA, within the present static LFC theory, and within the theory of Holas *et al.*[48] where dynamical local-field effects are partially accounted for by including the first-order corrections to the irreducible polarizability. Note that this first-order theory gives spurious singularities[50] at $z=|Q^2\pm Q|$. As indicated in Fig. 11, the present theory and the first-order dynamical theory agree quite well in terms of their corrections to the RPA dielectric function. As mentioned previously, both theories predict a decrease (compared to RPA) in the peak position of the energy-loss function, and this is seen in Fig. 12; however, the disparity between them is considerably larger than that observed in Fig. 11. As with the RPA-type theories, the first-order dynamical theory (at zero temperature) also fails to predict the experimentally observed nonvanishing energy-loss function in the high-frequency region $z>Q^2+Q$, where single particle-hole excitations are forbidden, but multipair excitations are not.

In summary, although the static LFC approximation of Eq. (2.16) represents a marked improvement over the RPA in terms of the thermodynamics it predicts, it does have some shortcomings in terms of its description of some of the high-frequency dielectric properties of the electron liquid. These errors are, however, diminished significantly by the frequency integrations required in calculating the free energy.

V. PAIR CORRELATION FUNCTION

Finally we analyze the pair-correlation function $g(r)$ of the electron liquid, defined by

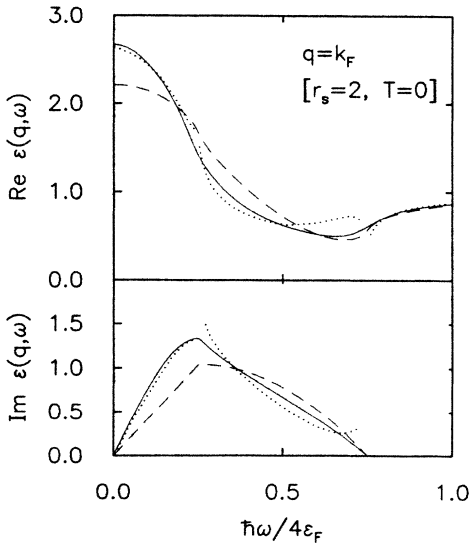

FIG. 11. Comparison of $\epsilon(q=k_F,\omega)$ at $r_s=2$ and $T=0$ in various theories. Solid curve is present theory, dashed curve is RPA, and dotted curve is from the dynamical LFC theory of Holas *et al.* (Ref. 48).

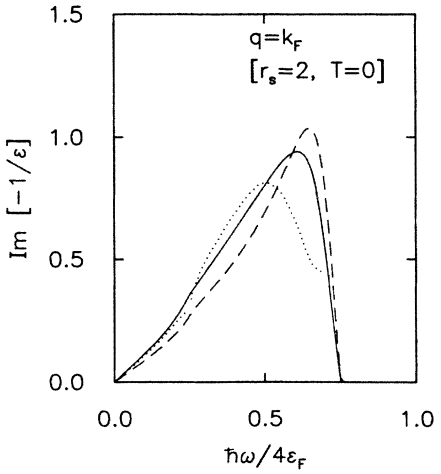

FIG. 12. Comparison of $\mathrm{Im}[1-/\epsilon(q=k_F,\omega)]$ in various theories at $r_s=2$ and $T=0$. Solid curve is present theory, dashed curve is RPA, and dotted curve is from the dynamical LFC theory of Holas *et al.* (Ref. 48).

$$g(r)=1+\frac{1}{n}\int\frac{d^3q}{(2\pi)^3}[S(q)-1]e^{iq\cdot r}\,, \tag{5.1}$$

where $S(q)$ is the static structure factor, related by the fluctuation-dissipation theorem to a frequency integral of the spectral function [see Eq. (2.14)]. In particular, we wish to show how $g(r)$ evolves from its degenerate form to its nondegenerate form as the temperature is increased. We will show how, even at large Θ where the classical results normally hold, quantum effects persist in $g(r)$ at small r.

Numerical evaluations of $S(q)$ from Eq. (2.14) have been performed, using the Padé approximant form of Eq. (4.8) for $\mathrm{Re}\chi_0(q,\omega)$. The results are shown (at $r_s=2$) for various degeneracy temperatures Θ in Fig. 13. The very small irregularities observable in some of the $S(q)$ curves at small q are numerical errors resulting from the compli-

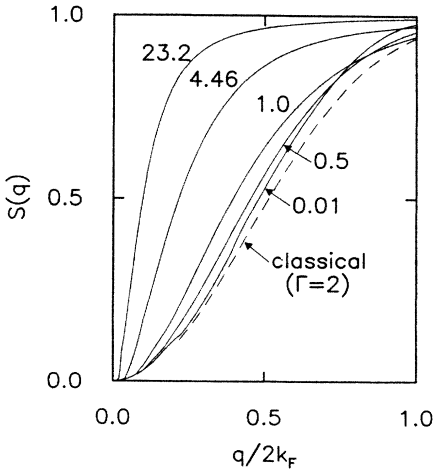

FIG. 13. Static structure factors as obtained from Eq. (2.14). Solid curves are for $r_s=2$; the degeneracy temperature Θ labels each curve. The dashed curve is the classical Monte Carlo result (Ref. 42) at $\Gamma=2$.

cation that the plasmon-pole and single-pair contributions to $S(q)$ no longer remain distinct at intermediate degeneracies. Specifically, the plasmon peak in $S(q,\omega)$ broadens from an approximate delta function at small q to a peaked structure with sufficient width that its contribution to $S(q)$ via the frequency integral of Eq. (2.14) can be evaluated numerically. Thus, for q less than a critical wave vector q_c (which decreases with temperature, as indicated in Fig. 9), we approximate the plasmon contribution to $S(q)$ as

$$S_{\rm plas}(Q)=\frac{6\pi Q^2}{\alpha r_s}\frac{[F_1^0(Q,z_p(Q))]^2}{\left|\frac{\partial}{\partial z}F_1^0(Q,z)\right|_{z=z_p(Q)}}, \tag{5.2}$$

where $F_1^0(Q,z)$ is given by (4.6) and (4.8), and $z_p(Q)$ is the plasmon dispersion. The small numerical errors mentioned above arise both from the inaccuracy in $\partial F_1^0/\partial z$ introduced by the Padé form (4.8), and from the inexact nature of the determination of q_c at nonzero temperatures. Note that the small Q behavior of (5.2) is

$$\lim_{Q\to 0} S_{\rm plas}(Q)=\frac{Q^2}{z_{p0}}[1-\tfrac{1}{2}A_2(r_s,\Theta)Q^2+\cdots], \tag{5.3}$$

where $A_2(r_s,\Theta)$ is defined by Eq. (4.11). This satisfies the exact long wavelength constraint on the plasmon contribution to $S(q)$.[6] Two further constraints on $S(q)$ that are also satisfied by our numerical evaluation of Eq. (2.14) are (i) that the single-pair excitations contribute[6] only to order q^5 at small q, and (ii) that the large q behavior of $S(q)$ is

$$\lim_{Q\to\infty} Q^4[S(Q)-1]=\frac{-\alpha r_s}{6\pi}(1-G_\infty), \tag{5.4}$$

where $G_\infty\equiv\lim_{q\to\infty}G(q)$.

The major feature of Fig. 13 is the manner in which $S(q)$ approaches unity more quickly for the higher-temperature plasmas. This is mainly attributable to the fact that the plasma becomes more weakly coupled as the temperature is increased at fixed density. (The coupling constant ζ ranges from 1.81 at $\Theta=0.01$ to 0.031 at $\Theta=23.2$.) To exemplify this point, we have also plotted in Fig. 12 the static structure factor for $\Gamma=2$ ($\zeta=1.33$) as obtained from classical Monte Carlo.[42] Note that the $\Theta=0.01$, $r_s=2$ curve and the classical $\Gamma=2$ curve have very similar values of ζ, and do indeed fall very near each other in Fig. 13.

In Fig. 14 are plotted the pair-correlation functions obtained by Fourier transforming the $S(q)$ curves of Fig. 13. In order to ensure accurate values of $g(r)$ at small r, the large Q contribution of the integral (5.1) is accounted for analytically by using

$$g(R)=1+12\int_0^{Q_{\rm max}}dQ\,Q^2[S(Q)-1]\frac{\sin(RQ)}{RQ}+\frac{\alpha r_s R}{10\pi}\left[Si(Q_{\rm max})-\frac{\cos(RQ_{\rm max})}{RQ_{\rm max}}-\frac{\sin(RQ_{\rm max})}{(RQ_{\rm max})^2}\right], \tag{5.5}$$

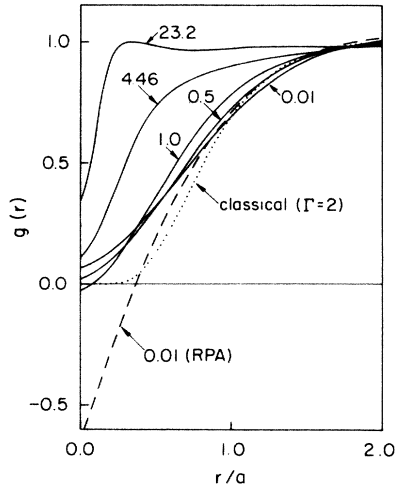

FIG. 14. Pair-correlation functions obtained through Fourier transform of the structure factors of Fig. 13. The degeneracy temperature Θ labels the solid (present calculations) and dashed (RPA) curves, all of which refer to plasmas with $r_s=2$. The dotted curve is the classical Monte Carlo result of Hansen (Ref. 13) at $\Gamma=2$.

where $R=2k_Fr$, $Q_{\rm max}$ is so chosen that for $Q>Q_{\rm max}$ the asymptotic form (5.4) holds, and the sine integral $Si(x)\equiv\int_x^\infty dt\,t^{-1}\sin(t)$ is obtained from numerical tables. We first note that the inclusion of local-field corrections does correct for the strongly negative values of the RPA $g(r)$ at small r. It is known, however, that even the present type of static LFC formulation still leads to negative values of $g(r=0)$ for sufficiently large r_s, due largely to the lack of self-consistency in the present theory.

The major effect of an increasing temperature on the pair-correlation functions plotted in Fig. 14 is the concomitant shrinkage of the exchange-correlation hole. Again, this is largely due to the decrease of the coupling constant ζ as Θ increases at fixed density. Note however, that since $S(Q=0)=0$ for all the curves in Fig. 13, there still remains exactly one excess charge in the exchange-correlation hole at all temperatures, and so the high-temperature $g(r)$ curves in Fig. 14 must contain more of a long-ranged contribution to the Coulomb hole than the degenerate curves. As in Fig. 13, we also plot the classical $\Gamma=2$ curve, obtained from the Monte Carlo calculations of Hansen,[13] in order that comparison can be made to the degenerate $r_s=2$ curve, which has a similar value of ζ. Note that although the small r behavior of the classical $g(r)$ is rather different from the degenerate case, for $r>a$ the two curves are quite similar.

Interestingly enough, the small r behavior of $g(r)$ is, in fact, largely dominated by quantum effects, even in plasmas that are otherwise quite classical. Note in Fig. 14, for example, that $g(r=0)$, after initially decreasing slightly to a minimum when $\Theta=1$ [due probably to the peaked structure in $\gamma(r_s,\Theta)$ at $\Theta\approx 1$; see γ_x in Fig. 3], then increases for the more weakly coupled high-temperature plasmas. [Note that we are here discussing the *output* value of $g(r=0)$; recall that on *input*, in Eq.

(2.20), we used $g(r=0)=0.1$. Again, the disparity between the two values reflects the lack of self-consistency in the present approach.] For $\Theta=23.2$, $g(0)\approx 0.3$, whereas for classical plasmas $g(0)$ vanishes identically. At $\Theta=23.2$ and $r_s=2$, however, our calculated excess free energy differs by less than 2% from its classical value. It can thus be seen how quantum effects are observable in the short-range pair-correlation behavior of a plasma that, for thermodynamic purposes, can be classified as classical. It is possible that for a real plasma with $\Theta \gg 1$ (but with $\hbar \neq 0$), there exists a critical distance within which the pair-correlation function crosses over from classical behavior [where $g(r=0)=0$] to quantum behavior [where $g(0)$ need not vanish]. Furthermore, this critical distance should decrease as Θ is increased. These purely quantum aspects of the very short-range correlations existing in otherwise classical plasmas may have some influence on, for example, the calculation of the enhancement rates for thermonuclear reactions.[51] No definite conclusions in this regard can be drawn from the preliminary results presented here, however.

VI. CONCLUSION

The goal of this work has been to present a unified theory, together with practical results, for the dielectric and thermodynamic properties of a one-component Fermi plasma throughout the full range of particle degeneracy. Through the inclusion of static local-field corrections, we have extended the range of validity of previous RPA theories from the weak coupling regime (where $\zeta \ll 1$) to the regime of intermediate coupling strengths ($\zeta < 10$). A major result of this work is the presentation of closed-form parametrizations of the free energy and dielectric function at any degeneracy; this should greatly enhance the utility of these calculations for practical applications. We also showed the qualitative and quantitative effects of both the local-field corrections and an increasing temperature on the dielectric function, particularly in terms of their effects on the plasmon dispersion and damping. Finally, we have studied the temperature effects on the pair-correlation function, and have shown how quantum effects can persist in the short-range correlations of an otherwise classical plasma.

APPENDIX

In this section we present the analytic fitting expressions that allow a closed-form description of the electron gas thermodynamic and dielectric properties as functions of density and temperature, as described in Sec. II. We begin by presenting the promised fits to the Fermi integrals $I_\nu(\eta_0)$ as functions of $\Theta=T/T_F$. By analyzing the low-temperature behavior of $I_\nu(\eta_0)$ via a Sommerfeld expansion, and the high-temperature behavior by a fugacity expansion, we are led to the following Padé approximants, valid for all values of Θ:

$$I_{-1/2}(\eta_0)\approx \frac{2}{\sqrt{\Theta}}\frac{1+c_1\Theta^2+c_2\Theta^4+c_3\Theta^6}{1+(c_1+\pi^2/12)\Theta^2+c_4\Theta^4+(c_3/\sqrt{2\pi})\Theta^{11/2}+(3c_3/2)\Theta^7}\,, \tag{A1}$$

$$I'_{-1/2}(\eta_0)\approx \sqrt{\Theta}\frac{1+c_1\Theta^2+c_2\Theta^4+c_3\Theta^7}{1+(c_1-\pi^2/6)\Theta^2+c_4\Theta^4+c_5\Theta^6+(3\sqrt{2}c_3/4\sqrt{\pi})\Theta^{15/2}+(3c_3/4)\Theta^9}\,, \tag{A2}$$

$$I_{3/2}(\eta_0)\approx \tfrac{2}{5}\Theta^{-5/2}\frac{1+c_1\Theta^2+c_2\Theta^4+c_3\Theta^8}{1+(c_1-5\pi^2/12)\Theta^2+c_4\Theta^4-(2c_3/15\sqrt{2\pi})\Theta^{11/2}+(2c_3/5)\Theta^7}\,, \tag{A3}$$

and

$$I_{5/2}(\eta_0)\approx \tfrac{2}{7}\Theta^{-7/2}\frac{1+c_1\Theta^2+c_2\Theta^4+c_3\Theta^{15/2}}{1+(c_1-7\pi^2/6)\Theta^2-(\sqrt{2}c_3/35\sqrt{\pi})\Theta^4+(4c_3/35)\Theta^{11/2}}\,. \tag{A4}$$

The constants c_i are given in Table I. The forms (A1)–(A3) are found to be accurate to within 0.1%, while (A4) is accurate to within 1%.

A convenient fitting expression for our calculated values of the correlation contribution to the electron gas free energy is (in rydbergs per electron)

$$f_c(r_s,\Theta)\approx \frac{\epsilon_c^0+d_1\Theta^2+d_2\Theta^3+d_3\Theta^4}{1+d_4\Theta^2+d_5\Theta^3-d_3(3r_s/8\alpha^2)^{1/2}\Theta^{9/2}}\,. \tag{A5}$$

Here $\epsilon_c^0(r_s)$ is a Hedin-Lundqvist type[43] of interpolation to our calculated zero-temperature correlation energy

$$\epsilon_c^0(r_s)\approx -0.0448[(1+y^3)\ln(1+1/y) + y/2-y^2-\tfrac{1}{3}]\,, \tag{A6}$$

where $y=r_s/20.52$, and the functions $d_j(r_s)$ are given by

$$d_1(r_s)=c_1+c_2r_s^{-c_3}\,, \tag{A7}$$

$$d_2(r_s)=c_1+c_2r_s^{-c_3}+c_4r_s^{-c_5}\,, \tag{A8}$$

$$d_3(r_s)=c_1+c_2r_s^{-c_3}+c_4r_s^{-c_5}\,, \tag{A9}$$

$$d_4(r_s)=\frac{c_1+c_2r_s+c_3r_s^2+c_4r_s^3+c_5r_s^4}{1+c_6r_s^2+0.022\,06r_s^5}\,, \tag{A10}$$

$$d_5(r_s)=(r_s+c_1)(c_2+c_3r_s^{-c_4})\,. \tag{A11}$$

The constants c_j are given in Table I. This match to f_c reproduces our calculations for all Θ and for r_s between 1 and 6 with a maximum error of 3%, and an average abso-

lute error of 0.5%. The largest errors in this parametrization occur for small Θ ($\Theta=0.05$ to 0.30), because the form (A5) neglects the weak $\Theta^2\ln(\Theta)$ singularity in f_c, known to cancel a similar singularity in the exchange free energy [see Eq. (2.12)]. Note that at large Θ it reduces to the Debye-Hückel form.

Finally, we present the closed-form-fitting expression used in Sec. IV to describe the electron gas polarizability. This is obtained by relating the interacting polarizability to the noninteracting one via Eq. (4.3), and using the Padé approximant for $\mathrm{Re}\chi_0(q,\omega)$ given by Eqs. (4.6)—(4.8). By analyzing the large x behavior of $\phi(x)$, the functions $b_j(\Theta)$ there are related to the functions $a_j(\Theta)$ by

$$b_{10}(\Theta)=\tfrac{3}{2}\sqrt{\Theta}I^0_{-1/2}a_8\ , \tag{A12}$$

$$b_8(\Theta)=\tfrac{3}{2}\sqrt{\Theta}I^0_{-1/2}a_6-\tfrac{1}{2}\Theta^{5/2}I^0_{3/2}b_{10}\ , \tag{A13}$$

and

$$b_6(\Theta)=\tfrac{3}{2}\sqrt{\Theta}I^0_{-1/2}a_4-\tfrac{1}{2}\Theta^{5/2}I^0_{3/2}b_8 -\tfrac{3}{10}\Theta^{7/2}I^0_{5/2}b_{10}\ , \tag{A14}$$

where we have set $I^0_\nu\equiv I_\nu(\eta_0)$. Similarly, the small x behavior of $\phi(x)$ implies that

$$b_2(\Theta)=a_2+2J(\Theta)/(3\sqrt{\Theta}I^0_{-1/2}) \tag{A15}$$

and

$$b_4(\Theta)=b_2^2-a_2b_2+a_4+2K(\Theta)/(15\sqrt{\Theta}I^0_{-1/2})\ , \tag{A16}$$

where

$$J(\Theta)\equiv-\int_0^\infty dx\,x^{-2}[f(x)-f(0)]\ , \tag{A17}$$

$$K(\Theta)\equiv-3\int_0^\infty dx\,x^{-4}[f(x)-f(0)-\tfrac{1}{2}x^2f''(0)]\ , \tag{A18}$$

and $f(x)\equiv[1+\exp(x^2/\Theta-\eta_0)]^{-1}$. Analysis at high and low temperature leads to the following approximations for $J(\Theta)$ and $K(\Theta)$:

$$J(\Theta)\approx\frac{1+c_1\Theta^2+c_2\Theta^4+c_3\Theta^7}{1+(c_1-\pi^2/6)\Theta^2+c_4\Theta^4+c_5\Theta^6+(3\sqrt{2}c_3/4\sqrt{\pi})\Theta^{15/2}+(3c_3/4)\Theta^9} \tag{A19}$$

and

$$K(\Theta)\approx\frac{1+c_1\Theta^2+c_2\Theta^4+c_3\Theta^7}{1+(c_1-3\pi^2/4)\Theta^2+c_4\Theta^4+c_5\Theta^7-(7\sqrt{2}c_3/8\sqrt{\pi})\Theta^{17/2}-(3c_3/8)\Theta^{10}}\ . \tag{A20}$$

Finally, the functions $a_i(\Theta)$ are expressed as

$$a_2(\Theta)\approx\frac{c_1+\Theta}{c_2+c_3\Theta^{c_4}+c_5\Theta^2}\ , \tag{A21}$$

$$a_4(\Theta)\approx\frac{1+c_1\Theta+c_2\Theta^2}{c_3+c_4\Theta+c_5\Theta^2+c_6\Theta^3+20.833c_2\Theta^4}\ , \tag{A22}$$

$$a_6(\Theta)\approx\frac{c_1+\Theta}{c_2+c_3\Theta+c_4\Theta^2+c_5\Theta^3+c_6\Theta^4}\ , \tag{A23}$$

and

$$a_8(\Theta)\approx\frac{0.91-6.4453\Theta+12.2324\Theta^2}{1+c_1\Theta+c_2\Theta^2+c_3\Theta^3+c_4\Theta^4+c_5\Theta^5+c_6\Theta^6}\ . \tag{A24}$$

The constants c_j in (A19)—(A24) appear in Table I. By testing this approximation for $\phi(x)$ over a wide range of Θ and x, the maximum error involved is found to be 2.5%, while the average error is less than 1%.

TABLE I. Fitting parameters used to describe the finite-temperature thermodynamic and dielectric properties of the electron gas. In the column marked c_j is the equation in which it appears.

c_j	$j=1$	$j=2$	$j=3$	$j=4$	$j=5$	$j=6$
(A1)	41.775	27.390	4287.2	50.605		
(A2)	2.2277	126.92	5248.0	97.720	861.30	
(A3)	5.3588	−2.5433	432.89	1.8800		
(A4)	−8.6164	−357.41	5711.1			
(A7)	0.144 59	−5.4210	0.900 23			
(A8)	−8.2583	11.196	0.130 12	12.308	2.2634	
(A9)	0.054 33	−11.196	2.0470	−6.8432	5.00	
(A10)	−328.63	316.63	99.064	8.0679	0.327 13	36.371
(A11)	−0.610 61	0.098 12	−15.633	1.6810		
(A19)	3248.8	−691.47	−3 202 700	−4535.6	−462 400	
(A20)	−4.8780	473.25	−2337.5	348.31	1517.3	
(A21)	−0.2280	0.4222	−0.6466	0.705 72	5.8820	
(A22)	−3.0375	64.646	19.608	−96.978	423.66	−331.01
(A23)	−0.1900	0.365 38	−2.2575	22.942	−43.492	106.40
(A24)	−7.1316	22.725	58.092	−436.02	−826.51	4912.9

ACKNOWLEDGMENTS

We wish to thank K. Runge, H. DeWitt, and L. Reatto for useful discussions, and J. Wang for his assistance with Fig. 1. This work was supported by the U.S. Army Research Office under grant number DAAG-29-82-K-0170 (work at Cornell University), and by the U.S. Department of Energy under Grant No. DE-FG02-84ER45130 (work at Washington University).

[1]These have appeared in abbreviated form in a preliminary account of this work, R. G. Dandrea and N. W. Ashcroft, in *The Proceedings of the 1985 APS Topical Conference on Shock Waves in Condensed Matter,* edited by Y. M. Gupta (Plenum, New York, 1986).

[2]H. E. DeWitt, J. Math. Phys. **3**, 1003 (1962).

[3]N. W. Ashcroft and D. Stroud, in *Solid State Physics,* edited by H. Ehrenreich, F. Seitz, and D. Turnbull (Academic, New York, 1978), Vol. 33, p. 1.

[4]S. Ichimaru, Rev. Mod. Phys. **54**, 1017 (1982).

[5]K. S. Singwi and M. P. Tosi, in *Solid State Physics,* edited by H. Ehrenreich, F. Seitz, and D. Turnbull (Academic, New York, 1981), Vol. 36, p. 177.

[6]D. Pines and P. Nozières, *The Theory of Quantum Liquids* (Benjamin, New York, 1966), p. 136.

[7]G. D. Mahan, *Many-Particle Physics* (Plenum, New York, 1981).

[8]K. S. Singwi, M. P. Tosi, R. H. Land, and A. Sjolander, Phys. Rev. **176**, 589 (1968).

[9]P. Vashista and K. S. Singwi, Phys. Rev. B **6**, 875 (1972).

[10]D. Ceperley, Phys. Rev. B **18**, 3126 (1978); D. M. Ceperley and B. J. Alder, Phys. Rev. Lett. **45**, 566 (1980).

[11]R. Abe, Prog. Theor. Phys. **22**, 213 (1959).

[12]Y. Rosenfeld and N. W. Ashcroft, Phys. Rev. A **20**, 1208 (1979); H. Iyetomi and S. Ichimaru, *ibid.* **27**, 3241 (1983).

[13]J. P. Hansen, Phys. Rev. A **8**, 3096 (1973); **8**, 3110 (1973).

[14]W. L. Slatterly, G. D. Doolen, and H. E. Dewitt, Phys. Rev. A **26**, 2255 (1982).

[15]F. Hensel, in *Physics and Chemistry of Electrons and Ions in Condensed Matter,* edited by J. V. Acrivos, N. F. Mott, and A. D. Yoffee (Reidel, Dordrecht, 1984), p. 401; G. Franz, W. Freyland, and F. Hensel, J. Phys. (Paris) Colloq. **41**, C8-70 (1980).

[16]B. Rozsnyai, Phys. Rev. A **5**, 1137 (1972).

[17]A. Mooradian, in *Proceedings of the International Conference on Light Scattering Spectra of Solids,* edited by G. B. Wright (Springer, New York, 1969), pp. 285–295.

[18]T. L. Reinecke, in *Polarons and Excitons in Polar Semiconductors and Ionic Crystals,* edited by J. T. Devreese and F. Peeters (Plenum, New York, 1984), pp. 343–382. The analysis of this paper is not directly applicable to the electron-hole liquid, however, since it must be treated as a two-component plasma.

[19]G. Chabrier and J. P. Hansen, J. Phys. C **18**, L757 (1985).

[20]M. A. Pokrant, Phys. Rev. A **16**, 413 (1977).

[21]U. Gupta and A. K. Rajagopal, Phys. Rev. A **22**, 2792 (1980).

[22]W. Stolzmann and W. D. Kraeft, Ann. Phys. (Leipzig) **36**, 388 (1979).

[23]M. W. C. Dharma-wardana and R. Taylor, J. Phys. C **14**, 629 (1981).

[24]F. Perrot and M. W. C. Dharma-wardana, Phys. Rev. A **30**, 2619 (1984).

[25]D. G. Kanhere, P. V. Panat, A. K. Rajagopal, and J. Callaway, Phys. Rev. A **33**, 490 (1986).

[26]C. Gouedard and C. Deutsch, J. Math. Phys. **19**, 32 (1978).

[27]N. R. Arista and W. Brandt, Phys. Rev. A **29**, 1471 (1984).

[28]S. Tanaka, S. Mitake, and S. Ichimaru, Phys. Rev. A **32**, 1896 (1985).

[29]A. L. Fetter and J. D. Walecka, *Quantum Theory of Many Particle Systems* (McGraw-Hill, New York, 1971), p. 231.

[30]B. Horovitz and R. Thieberger, Physica **71**, 99 (1974).

[31]Reference 6, p. 136.

[32]J. Hubbard, Proc. R. Soc. (London) **243**, 336 (1957).

[33]D. J. Geldart and S. H. Vosko, Can. J. Phys. **44**, 2137 (1966).

[34]N. Iwamoto and D. Pines, Phys. Rev. B **29**, 3924 (1984); N. Iwamoto, E. Krotscheck, and D. Pines, *ibid.* **29**, 3936 (1984).

[35]D. C. Langreth, Phys. Rev. **181**, 753 (1969).

[36]G. Vignale and K. S. Singwi, Phys. Rev. B **32**, 2156 (1985).

[37]D. Pines, in *Quantum Fluids,* edited by D. F. Brewer (North-Holland, Amsterdam, 1966), p. 257.

[38]Reference 6, p. 209.

[39]J. C. Kimball, Phys. Rev. A **7**, 1648 (1973).

[40]S. H. Vosko, L. Wilk, and M. Nusair, Can. J. Phys. **58**, 1200 (1980).

[41]K. Utsumi and S. Ichimaru, Phys. Rev. B **24**, 3220 (1981).

[42]K. Tago, K. Utsumi, and S. Ichimaru, Prog. Theor. Phys. **65**, 54 (1981).

[43]L. Hedin and B. I. Lundqvist, J. Phys. C **4**, 2064 (1971).

[44]H. E. DeWitt, J. Math. Phys. **3**, 1216 (1962).

[45]Reference 29, p. 303.

[46]D. G. Pettifor and M. A. Ward, Solid State Commun. **49**, 291 (1984).

[47]P. E. Batson, C. H. Chen, and J. Silcox, Phys. Rev. Lett. **37**, 937 (1976).

[48]A. Holas, P. K. Aravind, and K. S. Singwi, Phys. Rev. B **20**, 4912 (1979).

[49]E. Petri and A. Otto, Phys. Rev. Lett. **34**, 1283 (1975).

[50]These singularities have also manifested themselves in the results of an alternative scheme for including dynamical local field effects, which is based on a Hartree-Fock decoupling of the equation of motion for the Wigner distribution function. J. T. Devreese, F. Brosens, and L. F. Lemmens, Phys. Rev. B **21**, 1349 (1980); **21**, 1363 (1980). Later work [H. Nachtegaele, F. Brosens, and J. T. Devreese, Phys. Rev. B **28**, 6064 (1985)], however, has demonstrated how such singularities can be removed by an extension of this theory.

[51]H. E. DeWitt, H. C. Graboske, and M. S. Cooper, Astrophys. J. **181**, 439 (1973); H. Itoh, H. Totsuji, S. Ichimaru, and H. E. DeWitt, *ibid.* **234**, 1079 (1979).